Research Article

Musa Adamu*, Yasser E. Ibrahim, Omar Shabbir Ahmed, and Qasem A. Drmosh

Mechanical performance of date palm fiberreinforced concrete modified with nanoactivated carbon

https://doi.org/10.1515/ntrev-2022-0564 received February 18, 2023; accepted June 5, 2023

Abstract: Date palm fiber (DPF) is an easily processed, low cost, and accessible natural fiber. It has mostly been used in composites for non-structural applications. For DPF to be utilized in cementitious composites for structural applications, ways to reduce its harmful effect on compressive strength must be devised. Therefore, in this study, nano-activated carbon (NAC), due to its filler effects, was used as an additive to produce the DPF-reinforced concrete (DPFRC). To produce the DPFRC, 0, 1, 2, and 3% by cement weight of DPF and NAC were added. The fresh properties, strength, and microstructure of the concrete were examined. The findings revealed that DPF decreased the consistency, density, and compressive strength. Additionally, it increases the porosity in the concrete microstructure. The addition of up to 1% NAC significantly improved the compressive, flexural, and split tensile strengths of the concrete, while it decreased the harmful impact of up to 2% DPF on the DPFRC's strength. The split tensile and flexural strengths of the concrete were enhanced with the addition of up to 2% DPF without any NAC. The addition of up to 2% NAC densified the DPFRC's microstructure by refining and filling the pores generated by the DPF. The multivariable statistical models developed to estimate the mechanical properties of the DPFRC containing DPF and NAC were very significant with a very high degree of precision.

Qasem A. Drmosh: Interdisciplinary Research Center for Hydrogen and Energy Storage, King Fahd University of Petroleum and Minerals, Dhahran 31216, Saudi Arabia; Department of Materials Science and Engineering, King Fahd University of Petroleum & Minerals, Dhahran 31261, Saudi Arabia

Keywords: natural fiber, date palm fiber, nano-activated carbon, mechanical properties

1 Introduction

One of the best ways to achieve sustainability is by proper utilization of waste materials and natural resources for building and construction applications. In terms of the consumption of natural resources, the construction industry is the foremost. With concrete being the major construction material, which is believed to be the second most used material after water, its production involves huge quantities of material resources [1-3]. Concrete possesses excellent compressive strength but poor tensile strength and strain properties, and easily cracks when subjected to tensile or bending stresses. Methods have been devised to address this shortcoming of concrete by using reinforcement to form a composite structure called reinforced concrete. As steel reinforcement is an expensive material, the cost of buildings and construction are increased. Hence, innovations to boost the tensile and strain characteristics of the concrete were derived by several researchers, using admixtures, fibers, and supplementary cementitious materials to the concrete [4–7]. This will decrease the amount of reinforcement needed to produce a reinforced concrete structure and hence reduce the overall cost of construction [2,8]. Fibers are added to cementitious composites as the main or secondary reinforcement [9,10]. In terms of main reinforcement, fibers are added to thin-sheet products where normal steel reinforcements cannot be used. This type of thin-sheet product contains a high amount of cement with no coarse aggregate in the matrix. The fibers are used to enhance the toughness, impact resistance, and tensile strengths, and prevent crack development and propagation. When used as a secondary reinforcement, fibers are added for controlling crack development and its propagation induced by temperature changes or humidity increases the post-cracking load resistance caused by spalling or overload [11,12]. Different types of fibers ranging from

^{*} Corresponding author: Musa Adamu, Engineering Management Department, College of Engineering, Prince Sultan University, Riyadh 11586, Saudi Arabia, e-mail: madamu@psu.edu.sa

Yasser E. Ibrahim, Omar Shabbir Ahmed: Engineering Management Department, College of Engineering, Prince Sultan University, Riyadh 11586, Saudi Arabia

natural fibers and man-made (synthetic) fibers have been added to cementitious composites in a variety of sizes. The choice of fibers depends on the availability, cost, type of cementitious composites, and the need for enhancement of the composite properties. Some of the commonly used synthetic fibers include polypropylene fiber, polyethylene fiber, polyvinyl alcohol fiber, polyvinyl chloride fiber, steel fiber, glass fiber, and carbon fibers [12]. For natural fibers, they are sourced from natural resources like plants, vegetation, trees, and animals. Some of their attributes include low elasticity and high tensile strength [8,13]. Furthermore, natural fibers have some superior benefits when compared to synthetic and other fibers. These include environmental sustainability, low to zero cost, easy accessibility, lower density and abrasiveness, better resistance to alkalinity, and better thermal and acoustic properties [14,15]. Conversely, when compared to synthetic fibers, natural fibers have meager wettability and high absorption, and poor bonding with the cement matrix due to their hydrophilic nature [8,11].

Date palm fiber (DPF) is obtained from the tree of date palm. The date tree is one of the most common trees available in the Middle East countries like the Kingdom of Saudi Arabia [9]. The processed DPF can be used as a natural fiber in concrete. The DPF has been reported to enhance thermal insulation and acoustic properties and decrease the density of the composites [16,17]. Furthermore, the DPF was found to boost the toughness, tensile strength, impact, and crack resistance of the composites [8,11,18]. On the contrary, the key shortcoming of adding DPF in the cementitious composite is that it led to a decrease in the compressive strength, triggered by the hydrophilicity of the fiber, which reduced its bonding with the cement matrix and decreased the strength. DPF also increases the porosity in the microstructure of the composites due to air entrainment on its surface during mixing. DPF also decreased the consistency of the composites, which results in balling effects of the fiber in the fresh composite, triggering increased pore volume in the cement matrix [8,16]. Different procedures have been used to counteract the detrimental impacts of the DPF on the strength and porosity of the composites. Khelifa et al. [19] treated the DPF with an alkali (NaOH) before incorporating it into the mortar. The treatment procedure involved using three combinations of NaOH concentrations and immersion times. The NaOH concentrations were 1, 2, and 3%, while the immersion times were 2, 8, and 14 h. The optimum treatment was found to be a 5% NaOH solution with an immersion time of 8 h. They reported that the addition of 1% DPF treated with 5% NaOH for 8 h resulted in the enhancement of the compressive strength and modulus of elasticity of the mortar by 46.6 and 36.3%, respectively, when compared to the mortar in

which 1% untreated DPF was added. They attributed the enhancement in strength and modulus to the improvement in the surface roughness and removal of impurities from the DPF, which led to better bonding between the mortar matrix and DPF and hence improved the strength. In a similar study, Ozerkan et al. [11] treated the DPF using Ca(OH)2 and NaOH before utilizing it in concrete. They observed an increase in the compressive strength of the concrete when Ca(OH)2-treated DPF was added in a dosage of up to 2%. However, Ibrahim et al. [8] used a pozzolanic material in the concrete produced with DPF. They replaced cement with silica fume at dosages of 5, 10, and 15% by volume of cement in the concrete containing 1, 2, and 3% DPF. They concluded that the incorporation of up to 10% silica fume as a replacement to cement led to the total mitigation of loss in the compressive strength due to the undesirable impact of the addition of 1 and 2% DPF in the concrete.

Activated carbon (AC) is obtained from materials of carbonaceous sources, such as wood, coir, rick husk, coconut husk, coal, petroleum pitch, and lignite, and it is produced from either chemical or physical activation processes. There are several types of ACs, including granular, extruded, bead, powdered, polymer coated, and impregnated ACs. Powdered AC is processed from granular AC that has a large surface area and is very porous to be able to absorb chemical components like mercury [20,21]. ACs were used as cement additives in industrial applications as early as 1952 for the prevention of the contamination of oil-well linings when in contact with drilling muds [22,23]. ACs in powdered and granular form were used for different engineering applications: (a) as additives to cementitious materials in concrete for absorption of nitrogen oxides and other volatile organic compounds formed from combustion in parking garages and roadway tunnels; (b) as aggregates for production of lightweight concrete; (c) for the prevention of microbial-induced corrosion in concrete sewer pipelines; and (d) in self-healing concrete for the transport of bacteria to aid the self-healing process [23–28]. Powdered ACs due to their high porosity at the nanoscale and larger surface area make them good materials for the densification of the microstructure at nano levels [29]. AC in powdered form has been used as additives in concrete and mortar. Na et al. [30] reported improvement in the strength of mortar with the addition of up to 1.5% powdered AC. They also detected an increase in the strength hardening process with the inclusion of powdered AC, which led to the reduction in curing time. They found that 0.5% nano-activated carbon (NAC) significantly improved the early strength while 1.5% powdered AC improved the strength better at 28 days. Zheng et al. [31] also reported an increase in the compressive strength of fly ash mortar with the addition of NAC; from the microstructural analysis, they observed that powdered AC acted as a filler and densified the mortar microstructure, hence improving the strength. Wang et al. [32] added different proportions of powdered AC, between 0.5 and 2.0% by binder weight, in conventional cement mortar and mortar containing fly ash as a partial substitute to cement. They reported that the powdered AC had a very good dispersing ability in the cement matrix. The pore volume of the mortar with or without fly ash decreased with the addition of NAC due to its filler effect. Furthermore, the strength of the mortar increased while its water absorption decreased with the addition of powdered AC.

DPF is one of the cheapest and most easily processed natural fibers for use in cementitious composites, which is readily available, especially in the middle-east countries. DPF has been found to improve some properties of cementitious composites such as thermal insulation, acoustic properties, ductility, and energy absorption capacity. However, the primary impediment to utilizing DPF in cementitious composites is an increase in porosity and a decrease in the strengths of the composites. This led to its shortcomings when used in concrete, especially for structural applications. Different methods have been used to mitigate the adverse impact of the DPF in mortar and concrete, with some methods being ineffective and other methods being effective but expensive. With AC in powdered form, a cheaper material has been found to improve the mechanical strengths of concrete and mortar by densifying the microstructure and reducing the pore volume. However, even with a series of advantages listed, AC in powdered form has not been used in DPF-reinforced concrete (DPFRC) as there are scanty or no available studies that utilized powdered AC in DPFRC to minimize the adverse influence of the DPF. Therefore, in this study, powdered AC in nano size was used as an additive to the DPFRC to mitigate the negative effects of the DPF on the porosity and mechanical strengths of the concrete.

2 Materials and methods

2.1 Materials

In this research, ordinary Portland cement (OPC) was utilized as the main binder material. The OPC was of Type I and the chemical compositions are given in Table 1, which conformed with the standard requirements of ASTM C150/ 150M [33]. The cement has a specific gravity (SG) and bulk density of 3.15 and 1,440 kg/m³, respectively. The AC used was obtained in commercial quantity from the BMS factory

Table 1: Chemical compositions of cement

Oxides	Compositions (%)	NAC
CaO	65.18	0.53
Al_2O_3	5.39	0.64
Fe_2O_3	3.4	0.60
SiO ₂	19.17	1.57
MgO	0.91	_
TiO ₂	0.24	0.06
Na ₂ O	0.17	_
K ₂ O	1.22	0.06
P_2O_5	0.09	0.15
SO ₃	3.51	_
MnO	0.18	_
Carbon	_	91
Loss of ignition	2.38	

in Saudi Arabia. The AC was obtained in a granular form and then ground using a miller that is capable of grinding the AC up to sizes less than 38 µm. After grinding, the AC was sieved through a 38 µm (No. 400) sieve to obtain the powdered AC. The powdered AC was further subjected to dry milling to reduce it to nanoscale size. Milling was done using a Pulverisette 7 Premium planetary ball milling machine. The NAC has a mean pore diameter, bulk density, and specific surface area of 2.14 nm, 0.5 g/cm³, and 3,000 m²/g, respectively. Additionally, the iodine number of the NAC was found to be 950 mg/g and its ash content was 10%. Figure 1 shows the used AC in granular and nano forms.

A clean and dust-free natural river sand was employed as the fine aggregate. The fine aggregate has a fineness modulus, bulk density, and SG of 2.26, 1,565 kg/m³, and 2.63 respectively. Moreover, the aggregate was found to have water absorption and mud content of 1.87 and 1.1%, respectively. Figure 2 depicts the gradation curve of the fine aggregate, which was found to be within the specified range of ASTM C33 [34]. For the coarse aggregate, crushed granite was used. The aggregate was thoroughly washed in clean water to remove any form of impurity and dust. The aggregate has a maximum nominal size, SG, and bulk density of 19 mm, 2.67, and 1,455 kg/m^{3,} respectively. The gradation curve for the aggregate, as shown in Figure 2, is within the range required for coarse aggregate in concrete by ASTM C33 [34].

DPF was obtained from the mesh of the date palm tree in raw forms. The mesh was in interwoven form of length varying between 300 and 500 mm and width between 200 and 300 mm. The raw mesh was processed and reduced to single DPFs by carrying out the following steps: The mesh was separated by hand and then submerged in clean water and washed thoroughly. Then, the washed mesh was immersed in 3% NaOH solution for about 3 h to remove all forms of impurities and dirt. After that, the fiber mesh was thoroughly

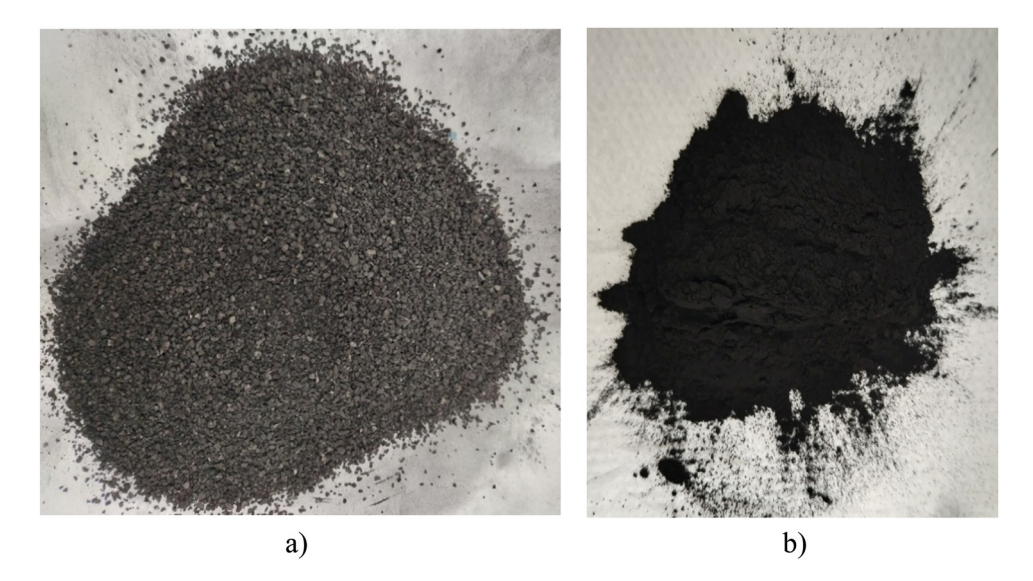


Figure 1: AC: (a) granular AC and (b) ground AC.

washed with clean water and then separated into single fibers of length varying from 20 to 30 mm and diameters from 0.2 to 1.0 mm. The single fibers were allowed to dry completely in the air for about 48 h before adding to the concrete. The fiber mesh and single fibers are shown in Figure 3, and the properties of the DPF are illustrated in Table 2.

2.2 Mixture proportions

The ACI 211.1R procedure [35] was followed for designing the concrete to obtain the constituent materials for the control mix. The volume of the superplasticizer was kept at 1% (by wt) to counteract the effects of variations in the w/c ratio throughout the mixes. The DPF was incorporated into the mixes at varying proportions of 1, 2, and 3% (by wt) of the binder. The NAC was used as an additive in the DPFRC and was incorporated at proportions of 1, 2, and 3% (by cement weight). Sixteen mixes including the control were obtained using different combinations of DPF and NAC, as presented in Table 3. Each of the mixes in Table 3 is designated a distinctive ID. Mix M1F1A is a mix with 1% DPF and 1% NAC; mix M0F2A is a mix with 0% DPF and 2% NAC; and mix M1F3A is a mix with 1% DPF and 3% NAC.

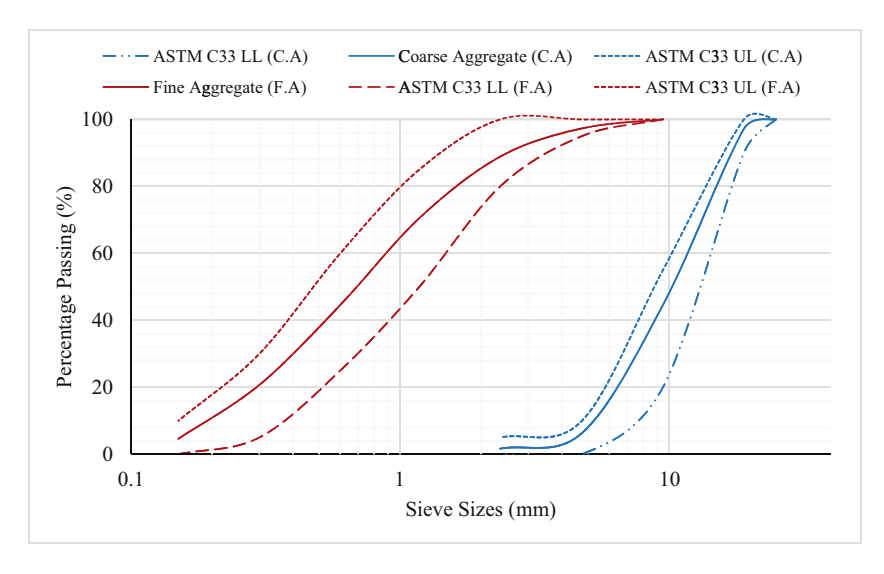


Figure 2: Particle size gradations of aggregates.



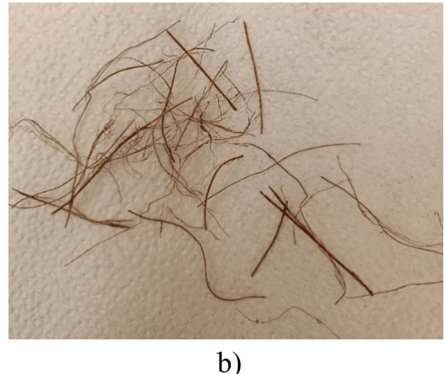


Figure 3: (a) DPF mesh and (b) single DPF.

Table 2: Properties of DPF

Properties	Units	Values		
Fiber length	mm	20-30		
DPF diameter	mm	0.2-1.0		
Bulk density	kg/m³	877.43 ± 4.8		
Elastic modulus	GPa	3.35 ± 1.5		
Tensile strength	MPa	203.24 ± 30		
Elongation at failure	%	13.5 ± 2		
Saturated water absorption	%	102.65 ± 3.3		
Natural moisture content	%	10.2 ± 0.4		

2.3 Sample preparation

The developed mix proportions were produced in the laboratory for testing. Each of the constituent materials

for the mix under consideration was weighed. The batching, mixing, and casting of the concrete samples were accomplished following the procedures outlined in ASTM C192/ C192M [21]. To avert the absorption of some portion of the mixing water by the aggregates, they were brought to a saturated surface dried condition before mixing. The cement used was also ensured to be free from agglomeration, impurity, and lumps. The mixing was carried out in a rotating drum concrete mixer, as shown in Figure 4a. The fine aggregate, NAC, and cement were emptied into the mixer and were then thoroughly mixed for about 45 s. The DPF and part of the mixing water combined with the superplasticizer were added gradually during mixing. The coarse aggregate and the remaining part of water combined with superplasticizer were added. The mixing progressed and was stopped after a completely homogenous mix was

Table 3: Mixture proportions

Mix no.	Quantities for 1 kg/m³ (kg/m³)										
	Cement	DPF	NAC	Fine aggregate	Coarse aggregate	Water	SP				
Control	480	0.0	0.0	730	890	180	4.8				
M1F0A	480	0.0	0	730	890	180	4.8				
M2F0A	480	4.8	0	730	890	180	4.8				
M3F0A	480	9.7	0	730	890	180	4.8				
M0F1A	480	14.5	4.8	730	890	180	4.8				
M1F1A	480	4.8	4.8	730	890	180	4.8				
M2F1A	480	9.7	4.8	730	890	180	4.8				
M3F1A	480	14.5	4.8	730	890	180	4.8				
M0F2A	480	0.0	9.6	730	890	180	4.9				
M1F2A	480	4.9	9.6	730	890	180	4.9				
M2F2A	480	9.8	9.6	730	890	180	4.9				
M3F2A	480	14.7	9.6	730	890	180	4.9				
M0F3A	480	0.0	14.4	730	890	180	4.9				
M1F3A	480	4.9	14.4	730	890	180	4.9				
M2F3A	480	9.9	14.4	730	890	180	4.9				
M3F3A	480	14.8	14.4	730	890	180	4.9				

6 — Musa Adamu et al. DE GRUYTER





Figure 4: Preparation of samples [8,36]: (a) mixing fresh concrete and (b) hardened samples.

obtained. Instantly following the mixing, the slump and fresh density of the fresh concrete were determined. The fresh concrete was then cast in the designated molds and kept in the laboratory for 24 h to settle and harden, as shown in Figure 4b. After hardening, they were removed from the molds and submerged in clean water for curing.

2.4 Test methods

The slump test was employed to measure the workability of the fresh concrete immediately after casting in accordance with ASTM C143/C143M [37] specifications. Afterward, the fresh density was measured following the guidelines listed in ASTM C138/C138M [38].

For testing the hardened properties, the compressive strength was measured after curing ages of 3, 7, and 28 days. Cubical samples of 100 mm sizes were produced and used for the testing in accordance with BS EN 12390-3 [39] specifications. The testing was done with the aid of a universal testing machine (UTM) of 2,000 kN capacity, as shown in Figure 5a. Similarly, the split tensile strength testing was done using the same UTM. Cylindrical samples of 200 mm height and 100 mm diameter were manufactured and subjected to curing for 3, 7, and 28 days before testing. Methods defined in BS EN 12390-6 [25] were adopted for the tensile strength testing. The test setup for the split tensile strength is shown in Figure 5b. The flexural strength testing was executed by adopting the procedures listed in ASTM C78/C78M [40]. Prismatic samples of 100 mm width, 100 mm height, and 500 mm length were manufactured and preserved for 7 and 28 days in water before testing. The flexural strength test was carried out using a UTM of 3,000 kN, as shown in Figure 5c. The water absorption test was done by following the methods explained in ASTM C78/C78M [40]. Cubical-shaped specimens of 100 mm dimensions were made and subjected to 28 days curing period before testing. Prior to testing, the samples were oven-dried for 24 h at 110°C as shown in Figure 5d. After oven drying, the weights of the samples were recorded and then the samples were completely immersed in clean water for another 24 h. The weights of the samples after immersion in water were recorded. The two measured weights were used to compute the water absorption.

The microstructural analysis was carried out on some selected samples. The microstructural morphology of the DPFRC was examined using a field emission scanning electron microscope (FESEM). Fractions of the concrete samples were obtained from the mixes after 28 days of curing. The fraction was completely dried and cleansed before coating with a thin gold film. The coated sample was inserted into the FESEM, and the morphology was captured using a high-resolution computer system. The morphology was captured at various resolutions between 1,000 and 10,000 magnifications and the best magnification was reported. The X-ray diffraction (XRD) test was carried out on some selected samples to determine the changes in the chemical composition, crystallinity, and structure of the DPFRC when NAC was added. An X'Pert3 MRD was used for the XRD test. Paste samples were extruded from the representative mixes after 28 days of curing. The pastes were then completely dried and cleaned before grinding to a fine nano form. The nanopaste samples were then placed in the machine, and the results were obtained

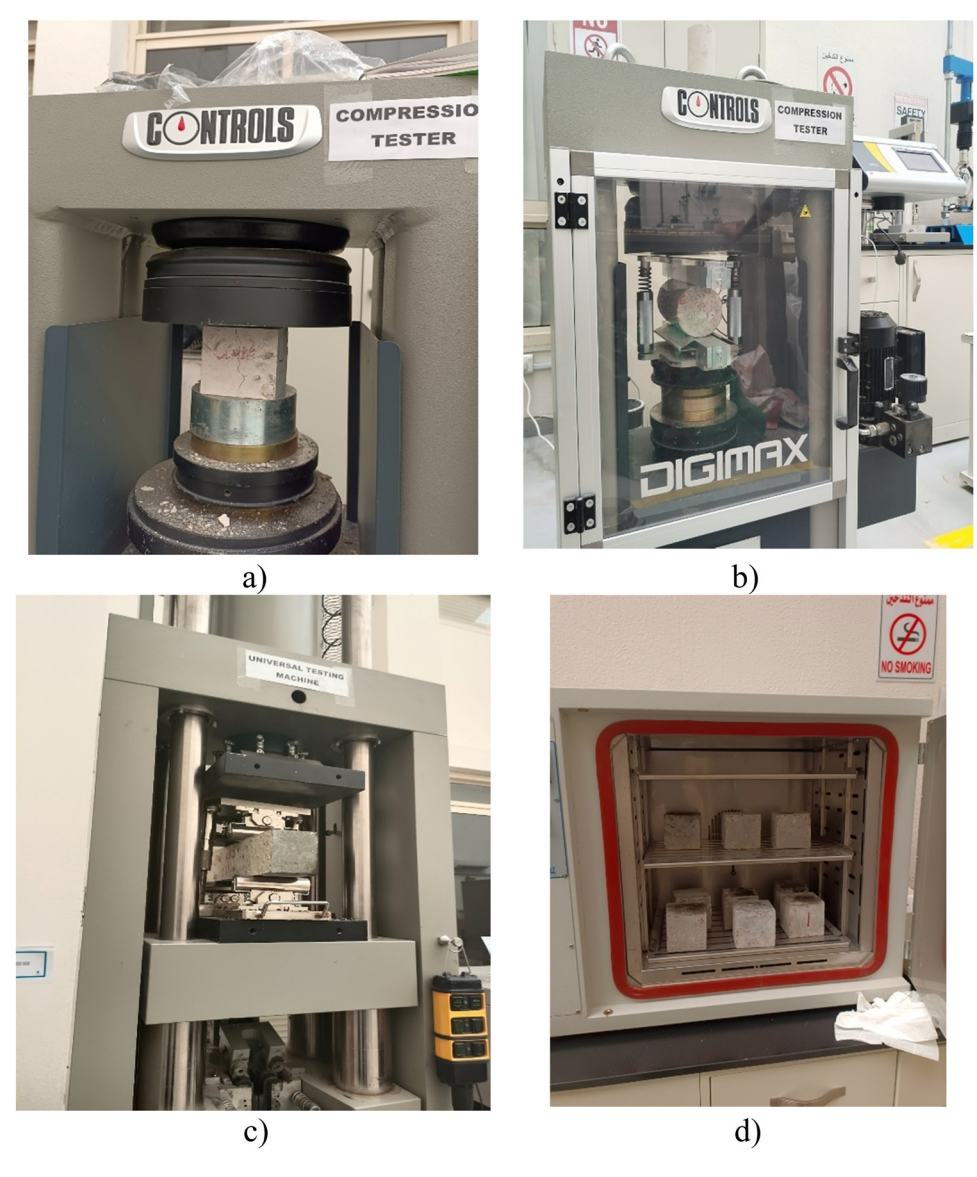


Figure 5: Testing methods: (a) compressive strength; (b) split tensile strength; (c) flexural strength; and (d) oven drying samples.

from the high-resolution computer system attached to the machine.

3 Results and discussion

3.1 Workability

The outcomes of the slump test for the DPFRC are presented in Figure 6. The slump values for all the mixes range between 84 and 50 mm. The addition of NAC caused a decrease in the slump values of the concrete. The slump values of mixes M0F1A, M0F2A, and M0F3A are 80, 65, and 55 mm, respectively, lower than that of the control, which

has a slump value of 84 mm. The decrease in slump values with the addition of NAC is because of its larger surface area, it absorbs more water to form a consistent paste and consequently reduces the workability. The high porosity of the NAC is owing to its larger surface area, which causes more friction in the fresh concrete mix, hence resulting in lower consistency [41]. The high loss of ignition of the NAC is owing to the carbon-based material, which also causes much absorption of mixing water thereby decreasing the fluidity and workability of the concrete. Similar outcomes have been observed by Rashad *et al.* [42] whereby they reported a decrease in flowability by up to 35% with the addition of up to 3.5% NAC to the alkali-activated paste. Lekkam *et al.* [41] also reported a decrease in the fluidity of the cement paste with the addition of 2% NAC. Zaid *et al.*

8 — Musa Adamu et al. DE GRUYTER

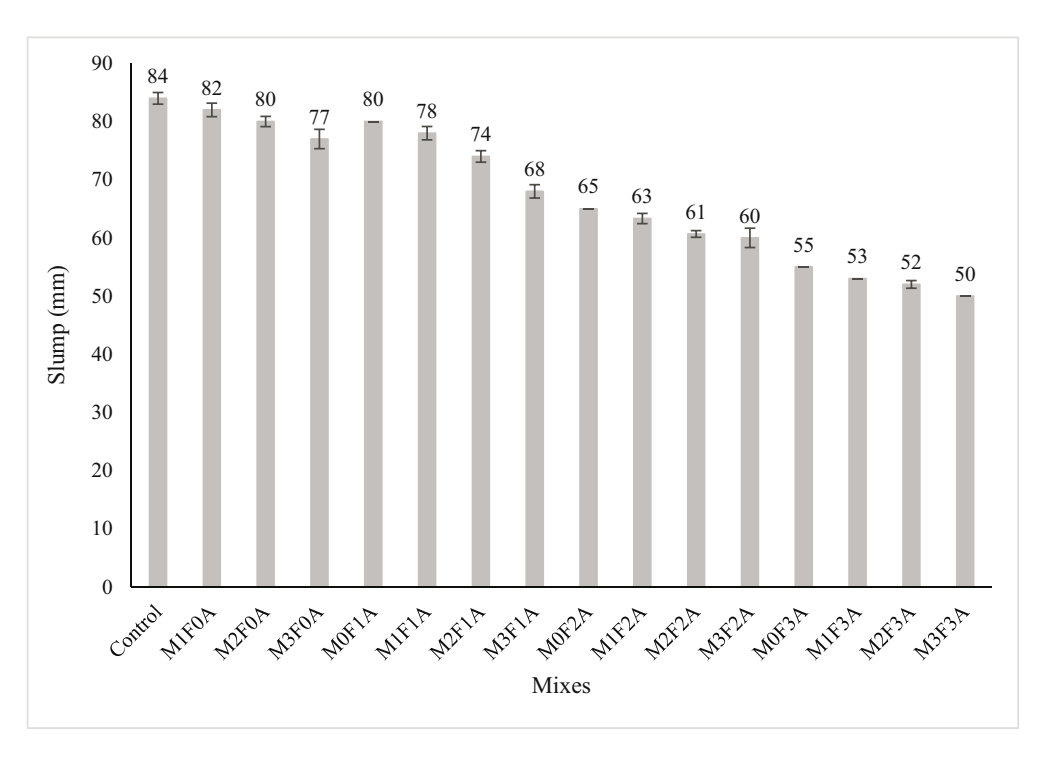


Figure 6: Results of the slump test.

[43] also reported that the workability of steel fiber-reinforced concrete decreased with the addition of graphene oxide to the concrete due to the larger surface area of the graphene material. The addition of DPF to the mixes containing different proportions of NAC caused a further decrease in the slump values as indicated in Figure 6. The slump values of M1F1A, M2F1A, and M3F1A were 78, 74, and 68 mm, respectively, compared to that for the mix M0F1A, which has a slump of 80 mm. The further decrease in the slump value with the addition of DPF is ascribed to the high hydrophilicity, porous structure, and lignocellulose and hemicellulose contents of the fiber, causing it to absorb parts of the mixing water and hence reducing the consistency of the fresh concrete mix [8,16,44]. From Figure 6, it is evident that the control mix has the highest slump of 84 mm, and the mix containing 3% DPF and 3% NAC (M3F3A) has the lowest slump of 50 mm. Therefore, to use both DPF and NAC in concrete it is recommended to add more amount of water-reducing admixtures like superplasticizers to counteract the decrease in consistency in the mix.

3.2 Density

The densities of the fresh and hardened mixes are presented in Figure 7. The density of the concrete slightly increased with the addition of up to 2% NAC. The fresh

densities of mixes M0F1A and M0F2A were higher by 0.7 and 1.1%, respectively, compared with the control. Comparable result trends can be seen for the density of the hardened mix also. The increase in density might be because NAC can serve as a filler material in the mix as a result of its large surface area, hence densifying the fresh mix and leading to an increase in density. Additionally, as NAC is used as an additive, it, therefore, increases the amount of constituent materials in the mix, which consequently increases the density/unit weight [45]. On the other hand, the addition of 3% NAC caused a decrease in the density of both the concretes, and this might be due to a great decrease in consistency, which cause agglomeration of the NAC leading to air entrainment and consequently a decrease in density. Incorporating up to 2% DPF into the concrete mixes containing up to 2% NAC led to an increase in the density of fresh and hardened mixes. For instance, in mixes consisting of 1% NAC in comparison to the control mix, the fresh densities of mixes M0F1A, M1F1A, and M2F1A were higher by 0.7, 1.1, and 1.5%, respectively. A similar result trend can be observed for the hardened mix. Equally, mixes containing 2% NAC have higher fresh density compared to the control mix by 1.1, 1.3, and 1.8% for mixes M0F2A, M1F2A, and M2F2A, respectively. The increase might be because DPF increases the volume of constituent materials in the mix, hence leading to higher density. Furthermore, the NAC due to its finer sizes fills the pores created by

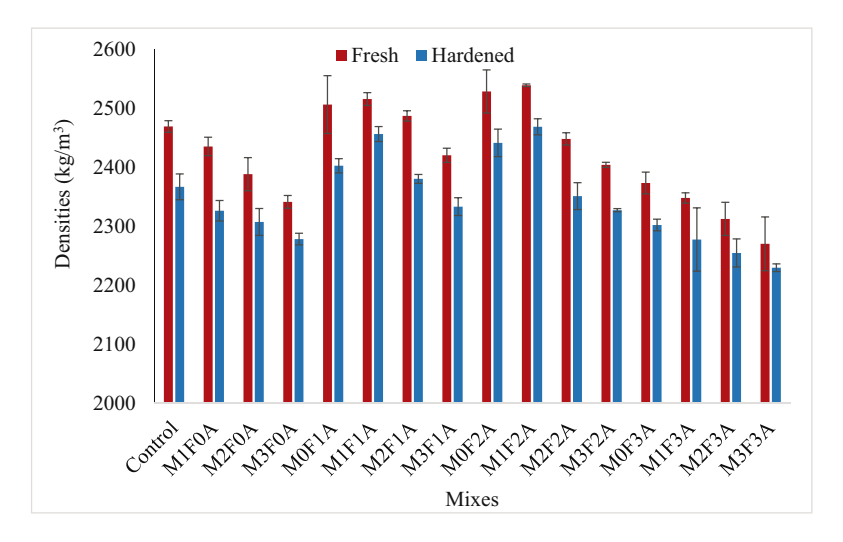


Figure 7: Results of densities of the fresh and hardened mixes.

the DPF in the cement matrix, hence densifying the paste which results in improved density. Though the addition of DPF to the concrete mixes containing 3% NAC caused a decrease in the fresh density. The fresh densities of the mixes with 3% NAC, *i.e.*, M0F3A, M1F3A, M2F3A, and M3F3A, were lower by 3.9, 5.3, 6,1, and 8.6%, respectively comparable to the control. This decrease in density might be due to the poor consistency of the mix, which causes agglomeration of the NAC and balling effects of the DPF, which causes a lot of air to be entrained in the fresh mix and consequently decrease in the density.

3.3 Compressive strength

Figure 8 depicts the compressive strengths for the DPFRC. The compressive strength decreases with the increase in the percentage of DPF added at all ages. Compared to the control at 7 days, the compressive strengths of mixes M1F0A, M2F0A, and M3F0A were lower by 6.54, 10.67, and 27.82%, respectively. Similarly, at 28 days, the compressive strengths of mixes M1F0A, M2F0A, and M3F0A were lower by about 5.48, 9.36, and 23.83%, respectively, compared to the control mix. The decrease in compressive

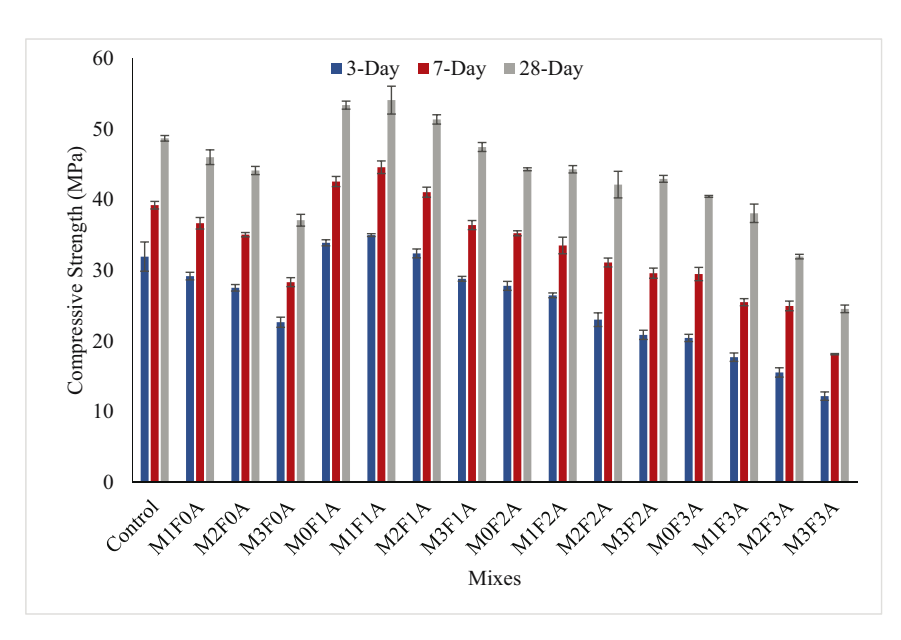


Figure 8: Compressive strength results.

strength with the addition of DPF was reported by other studies [8,46,47]. The decrease in the compressive strength was caused by the hydrophilic nature of the DPF, causing it to absorb part of the mixing water and decreasing the consistency of the mix. This led to the formation n of honeycombs and porosity in the composite matrix and consequently leading to premature failure and a decrease in strength. Moreover, the poor adhesion between the cement paste and DPF also contributed to the decrease in strength [8,46,47].

The addition of NAC to the DPFRC improved its compressive strength. For the mix containing 0% DPF, the addition of 1% NAC improved its compressive strength at all ages, where the compressive strengths of M0F1A improved at 3, 7, and 28 days by 6.15%, 8.53%, and 5.48% respectively, when compared with that of the control mixes at same ages. For the mixes with DPF, 1% NAC addition was successful in alleviating the loss in the compressive strength when 1 and 2% DPF were incorporated. For instance, the compressive strengths of mix M1F1A were superior to the control mix by 9.55, 13.7, and 11.12% at 3, 7, and 28 days, respectively. Similarly, the compressive strengths of mix M2F1A were more than that of the control mix by 1.44, 4.69, and 5.5%, at 3, 7, and 28 days, respectively. These results are consistent with the outcomes of previous studies where they reported an increase in compressive strength when 0.5% NAC [41] and up to 1.5% NAC was added [30,42]. The increase in the compressive strength of DFPRC with the addition of NAC was ascribed to the larger surface area and filler ability of the NAC, thereby filling the pores and air voids triggered by the DPF and densifying the concrete matrix and hence increasing the strength [42]. Another reason for the increase in strength might be due to the acceleration of the strength hardening process in the cement matrix by the NAC [30]. In a similar study, Maglad *et al.* [48] also reported that graphene oxide acted as a filler due to its larger surface area and increased compressive strength of the geopolymer concrete.

The addition of more than 1% NAC to the concrete with or without any DPF resulted in a decrease in the compressive strength at all ages. For the mixes without DPF, the compressive strengths of mix M0F2A were lower by 12.97, 10.16, and 9.01% at 3, 7, and 28 days, respectively, compared to the control mixes. Likewise, for the M0F3A mix, its compressive strengths were lower by 36.08, 24.88, and 16.9% at 3, 7, and 28 days, respectively, compared to the control. The decrease in the compressive strength is due to the interruption in the hydration of tricalcium aluminates by lowering its hydrolysis and formation of ettringites caused by the retarding effects of the carbon. Additionally, the impurities present in the NAC from its high iodine number, unburnt carbon, and other elements formed in the AC during its production might attenuate the hydration process and cause a decrease in its strength [41]. Furthermore, the finer sizes of NAC make it absorb some portion of the mixing water and decrease the workability of the fresh concrete. This led to poor compaction and balling effects of the fibers, increasing the pore volume in the hardened concretes' microstructure. This creates many weak paths for premature failure with load applications and consequently lower compressive strength.

3.4 Flexural strength

Figure 9 presents the flexural strengths for the DPFRC produced with different proportions of DPF and NAC. The

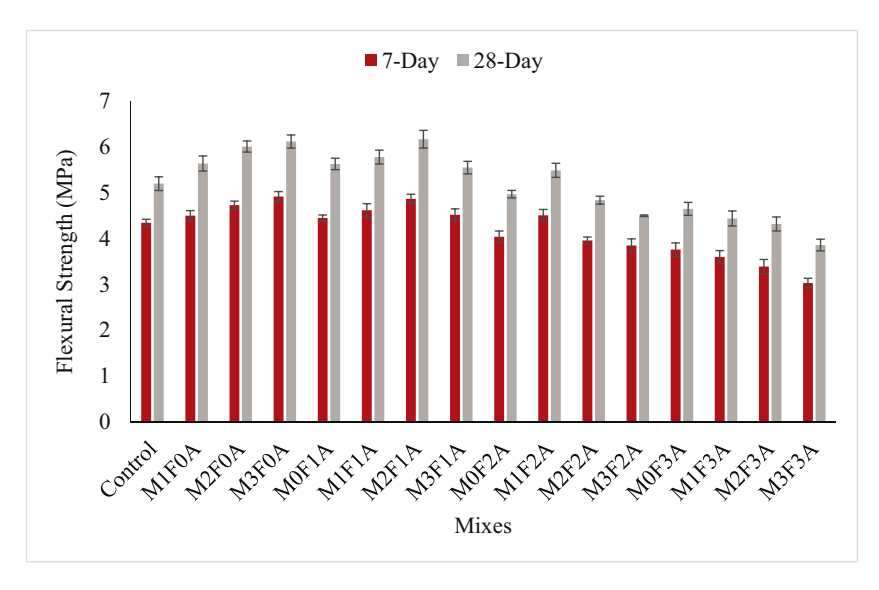


Figure 9: Flexural strength results.

flexural strength increased with the increase in the volume of DPF. In comparison to their respective control mixes, the flexural strength of mix M1F0A improved by 3.6 and 8.5% at 7 and 28 days, respectively, while for mix M2F0A its flexural strength improved by 8.9 and 15.6% at 7 and 28 days, respectively, likewise for mix M3F0A its flexural strength enhanced by 13.3 and 17.7%, respectively. The enhancement in flexural strength was credited to the fibrous nature of the DPF, resulting in the prevention and prolonging of crack spread and improving the bending resistance even after the first crack has occurred. Similar findings have been reported by previous studies [8,49].

The addition of 1% NAC to the mixes without DPF improved its flexural strength, where the strength of mix M0F1A enhanced by 2.44 and 8.3% at 7 and 28 days, respectively, compared to the control. The pore-filling effects of the NAC might be the reason for the upgrading in flexural strength [32]. The addition of 1% NAC further enhanced the flexural strengths of the DFPRC containing 1, 2, and 3% fibers. This is testified by comparing the flexural strengths of mixes M1F1A, M2F1A, and M3F1A with the control or respective mixes M1F0A, M2F0A, and M3F0A. The flexural strength of mixes M1F1A improved by 6.4 and 11.2% at 7 and 28 days, respectively, when match with the control mix. Similar result trends can be seen for mixes M2F1A and M3F1A. The addition of 2% NAC only enhanced the flexural strength of the mix with 1% DPF. This can be seen by comparing the flexural strength of mix M1F2A with that of the control, where the former has higher strength by 3.8 and 5.6% at 7 and 28 days, respectively, comparable to the former. The upgrade can be due to the

combination of crack bridging ability by the fiber and pore filling ability of the NAC. Conversely, the addition of 2% NAC to DPFRC containing 2 and 3% DPF resulted in a decrease in flexural strength as seen in Figure 9. Furthermore, the addition of 3% NAC to DPFRC containing 1, 2, and 3% DPF also led to a decrease in flexural strength. From all the mixes, the concrete with 3% DPF and 3% NAC (M3F3A) has the lowest flexural strength, where its strength decreased by 30.3 and 25.8% at 7 and 28 days, respectively, when compared with the control. The decrease in flexural strength with the addition of NAC to the DPF concrete was credited to the reduction in consistency which caused fiber balling in the fresh concrete. After the DPFRC has hardened, this lower consistency caused an increase in pore volume and air voids in the microstructure. This weakens the cement paste and creates a lot of weak paths for easy crack initiation and propagation and consequently resulting in a decrease in flexural strength.

3.5 Splitting tensile strength

Figure 10 summarizes the results of the split tensile strength for the DPFRC. The addition of up to 2% DPF led to an increase in tensile strength at all periods. Mix M1F0A has superior tensile strengths of about 5.8, 3.6, and 5.9% at 3, 7, and 28 days respectively, compared to the control. Similarly, mix M2F0A has greater tensile strengths at 3, 7, and 28 days by 7.7, 10.1, and 10.9%, respectively, compared to the control. The reason for the improvement in tensile strengths with

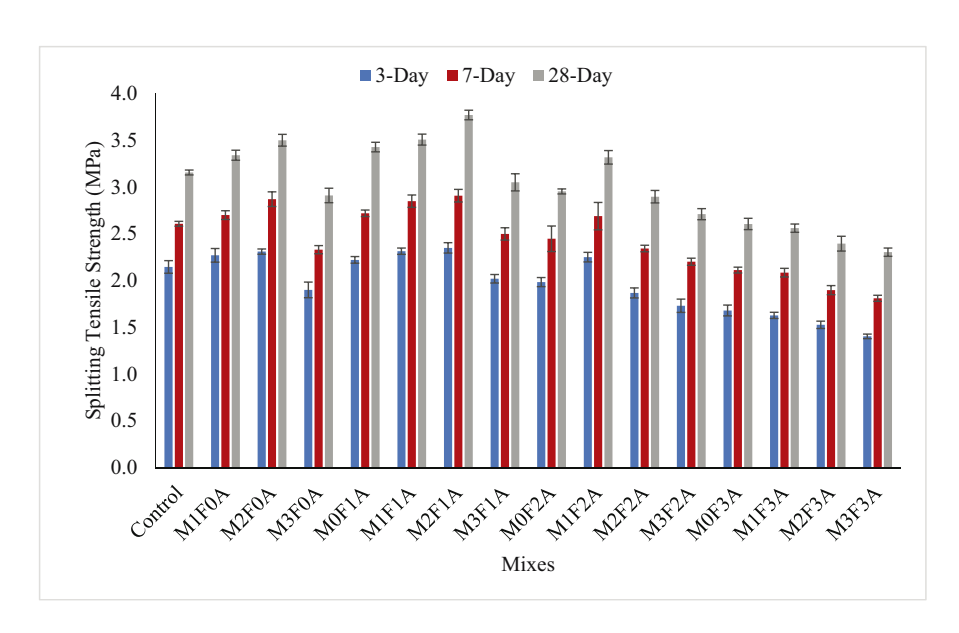


Figure 10: Results of splitting tensile strengths.

the addition of DPF may be due to the enhancement in the crack bridging effect and energy transfer mechanism by the fiber, which improved the post-crack failure resistance and increased the tensile strength [8].

The effect of NAC on the splitting tensile strength of the DPFRC is shown in Figure 10. The addition of 1% NAC to the plain concrete (without DPF) increased its splitting tensile strength at all ages. For instance, the tensile strength of M0F1A was superior to that of the control by 3.5, 4.3, and 8.6% at 3, 7, and 28 days, respectively. The increase in the tensile strength might be due to the decrease in the pore volume and air voids in the concrete's microstructure with the addition of NAC due to its filler ability. This consequently led to better gluing between the cement matrix and aggregate and thus improved the tensile strength. The addition of up to 2% NAC to the concrete containing 1 and 2% DPF led to further augmentation in the tensile strength. In comparison to the control, M1F1A has superior tensile strength by 7.9, 9.3, and 11.1% at 3, 7, and 28 days, respectively. Similarly, M2F1A has improved tensile strength by 9.5, 11.5, and 19.5% at 3, 7, and 28 days, respectively, when compared with the control. Finally, M1F2A has its tensile strength improved at 3, 7, and 28 days by 4.9, 3.1, and 5.1%, respectively, when compared with the control. This further increase in the tensile strength with the addition of NAC to the DPFRC is due to the combined influence of both the DPF and NAC. The NAC filled the pores generated by the DPF and consolidated the concrete's microstructure, thereby enriching the bonding between the fiber and paste, which resulted in increased tensile strength. However, the addition of 2 and 3% NAC led to a decrease in the split tensile strength of both the plain concrete (without DPF) and the DPFRC. For instance, the split tensile strengths of mix M0F2A at 3, 7, and 28 days were lower by 7.5, 6.1, and 6.2%, respectively, comparable to the control. Also, the tensile strengths of M0F3A at 3, 7, and 28 days were lower by 21.7, 19, and 17.5%, respectively. A further decrease can be seen with the addition of 2 and 3% NAC to the DPFRC with different proportions of DPF. At 3 days, the split tensile strengths of mixes M2F2A, M3F2A, M1F3A, M2F3A, and M3F3A were lower by 13, 19.3, 24.1, 28.8, and 34.6%, respectively, when compared to the control (at 3 days). However, at 28 days, the split tensile strengths of M2F2A, M3F2A, M1F3A, M2F3A, and M3F3A were lower by 8.2, 14.1, 18.9, 24.1, and 27%, respectively, compared to the control at the same age. The decrease in the tensile strength with the addition of NAC is caused by the significant decrease in consistency of the fresh concrete where both DPF and NAC absorb part of the mixing water. This instigated poor compaction and dispersion of the fibers in addition to balling effects of the fiber. This affected the hardened cement matrix by increasing the poor volume and air

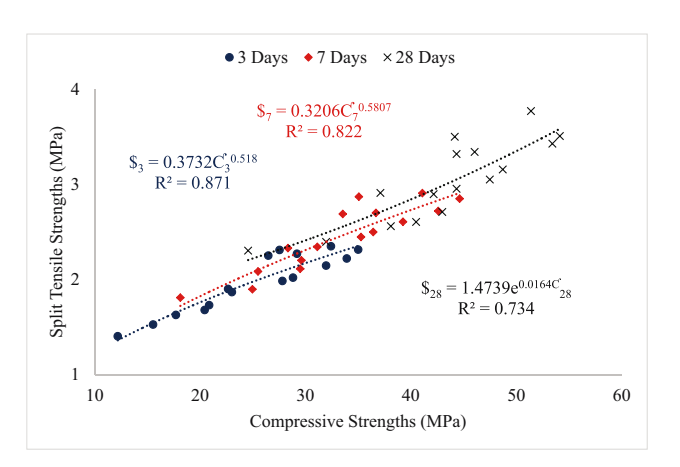


Figure 11: Relationship between compressive and split tensile strengths of DPFRC.

voids. Therefore, untimely failure arises through the weak paths and hence a decrease in the tensile strength.

3.6 Relationship between compressive strength and split tensile/flexural strengths

The relationships between compressive strength and split tensile strengths of the DPFRC containing different proportions of DPF and NAC are presented in Figure 11, while the relationship between the compressive strengths and flexural strengths is shown in Figure 12. In the figures, \mathcal{C} represents compressive strengths, \mathcal{C} represents split tensile strengths, and \mathcal{C} represents flexural strengths. A good correlation exists between the compressive strength and split tensile strength at 3, 7, and 28 days, as shown in Figure 11, as the strength relationships at all ages have a degree of correlations (\mathcal{C}) greater than 0.7, with the relationship at 3 days having the

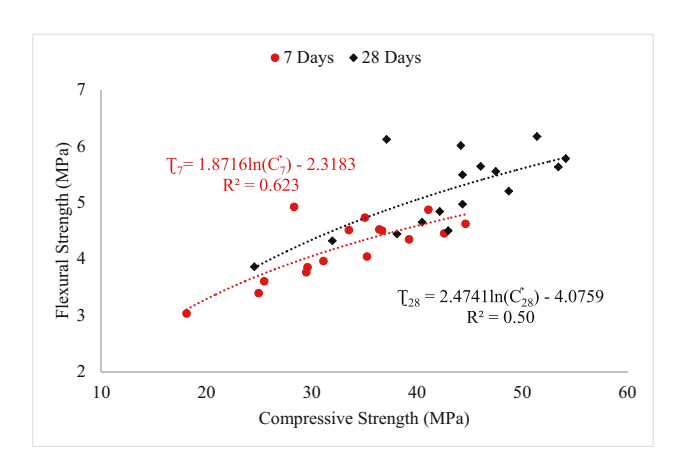


Figure 12: Relationship between compressive and flexural strengths of DPFRC.

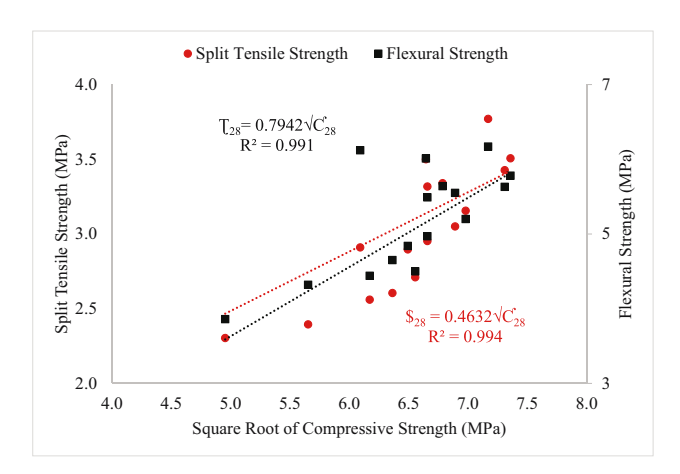


Figure 13: Power relationship between compressive strength and split tensile/flexural strengths.

best correlation. For the relationship between the compressive strengths and flexural strengths of the concrete at 7 and 28 days, as seen in Figure 12, a fair correlation existed as the strength relationships have R^2 values greater than or equal to 0.5, with the relationship at 28 days having the best degree of correlation. The splitting tensile strengths and flexural strengths at all ages were found to be directly proportional to their corresponding compressive strengths at the same ages.

Power relationships, which were proposed by ACI 318 [50] for the relationships between compressive strength and split tensile/flexural strengths of concrete, were developed and are presented in Figure 13 for the 28 day strengths.

All the strength relationships have excellent correlations, as both the compressive strength - split tensile strength and compressive strength - and flexural strength models have R^2 values greater than 0.99. Therefore, the power model is the best fit for predicting the split tensile and flexural strengths of the DPFRC using its compressive strengths compared to the other models developed in Figures 11 and 12. The power models developed in this study between the 28 days compressive strength and 28 days split tensile strengths were compared with already existing modes from ACI 318 [50], CEB-FIB [51], ACI 363 [52], and Hesami et al. [53], as shown in Table 4. Similarly, the developed model for the relationship between the 28-day compressive strength and the 28-day flexural strength was compared with the already existing models from ACI 318 [50], BS 8110, and Ahmed et al. [54], as shown in Table 4. The developed relationship between the compressive strength and split tensile strength of the DPFRC is close to the model proposed by ACI 318 [50], while the developed model for the compressive-flexural strengths relationship for the DPFRC is closer or similar to the model proposed by Ahmed et al. [54].

3.7 Water absorption

Figure 14 displays the water absorption results for the DPFRC containing different proportions of NAC and DPF. The water absorption increased with the increase in DPF.

Table 4: Comparison between the predicted strengths and existing models

Compressive strength		Split te	nsile strength		Flexural strength				
	This study	ACI 318 [50] $\$ = 0.56\sqrt{C'}$	CEB-FIB [51] \$ = 0.3 <i>C</i> ^{0.66}	Hesami et al. [53]	This study	ACI 318 [50] $T = 0.62\sqrt{C}$	BS 8110 [55] $T = 0.6\sqrt{C'}$	Ahmed et al. [54] 0.45C ^{2/3}	
		•		•			•		
48.71	3.16	3.91	3.90	3.49	5.20	4.33	4.19	6.00	
46.04	3.34	3.80	3.76	3.39	5.64	4.21	4.07	5.78	
44.15	3.50	3.72	3.65	3.32	6.01	4.12	3.99	5.62	
37.10	2.91	3.41	3.26	3.05	6.12	3.78	3.65	5.01	
53.42	3.43	4.09	4.14	3.65	5.63	4.53	4.39	6.38	
54.13	3.51	4.12	4.18	3.68	5.78	4.56	4.41	6.44	
51.39	3.77	4.01	4.04	3.58	6.17	4.44	4.30	6.22	
47.48	3.05	3.86	3.83	3.45	5.55	4.27	4.13	5.90	
44.32	2.95	3.73	3.66	3.33	4.97	4.13	3.99	5.64	
44.32	3.32	3.73	3.66	3.33	5.49	4.13	3.99	5.64	
42.15	2.90	3.64	3.54	3.25	4.84	4.03	3.90	5.45	
42.96	2.71	3.67	3.59	3.28	4.50	4.06	3.93	5.52	
40.48	2.60	3.56	3.45	3.18	4.65	3.94	3.82	5.31	
38.09	2.56	3.46	3.31	3.09	4.44	3.83	3.70	5.09	
31.95	2.39	3.17	2.95	2.83	4.32	3.50	3.39	4.53	
24.53	2.30	2.77	2.48	2.48	3.86	3.07	2.97	3.80	

The water absorption values of mixes M1F0A, M2F0A, and M3F0A were higher by 6.6, 14.2, and 25.6%, respectively, when compared with that of the control. The related outcomes were reported by Bamaga [56] and Ibrahim et al. [8]. The increase in water absorption was attributed to the hydrophilicity of the DPF owing to its high lignocellulose contents, which makes it absorb water during mixing. After the concrete dries, this creates excess pores in the hardened cement paste and thus increases absorption [8,57]. The addition of up to 2% NAC to the plain concrete (without DPF) led to a decrease in its water absorption. The water absorption values of M0F1A and M0F2A were lower by 20 and 9.9%, respectively, when compared to that of the control. The decrease in water absorption is attributed to the densification of the cement matrix by the finer particles of the NAC. The addition of up to 2% NAC lowered the water absorption of the DFFRC containing 1% DPF only. That is, the addition of up to 2% NAC cushioned the detrimental effect of 1% DPF addition on the water absorption of DPFRC. The water absorption values for M1F1A and M1F2A were lower by 12.1 and 7.9%, respectively, when compared to that of the control. The decrease in water absorption is due to the densification of the microstructure with the addition of NAC and reducing its porosity generated due to DPF inclusion, hence lowering its water absorption. On the contrary, the addition of more than 2% NAC led to a further increase in the water absorption of the plain concrete (without DPF) and the DPFRC. This was attributed to the adverse influence of the NAC on the consistency and fluidity of the fresh DPFRC, which resulted in difficult compaction and dispersal of the fiber, and hence intensified the porosity and air voids in the concrete's microstructure. This led to an increase in porosity and water absorption in the DPFRC.

3.8 Microstructural evaluation

3.8.1 **FESEM**

The influence of NAC as an additive and DPF on the microstructural properties of the DPFRC was examined using an SEM. Figure 15 presents the microstructural morphologies of the control mix and some mixes containing DPF and NAC. Scattered pores and microcracks can be detected on the concrete mix's surface as depicted in Figure 15a, with the microstructure relatively densified due to cement hydration. The scattered pores on the microstructure of the control might be due to air bubbles entrapped during mixing which dries up and creates voids in the matrix. As shown in Figure 15b, the microstructural morphology of mix M2F0A is the least densified and most porous. This is due to the adverse effect of the DPF resulting from its hydrophilic nature, whereby it absorbs water during mixing and entrains air on its surface. Drying, thereafter, led to more porosity in the microstructure [8]. The addition of NAC to the DPFRC densified its microstructure and filled up the surplus pores

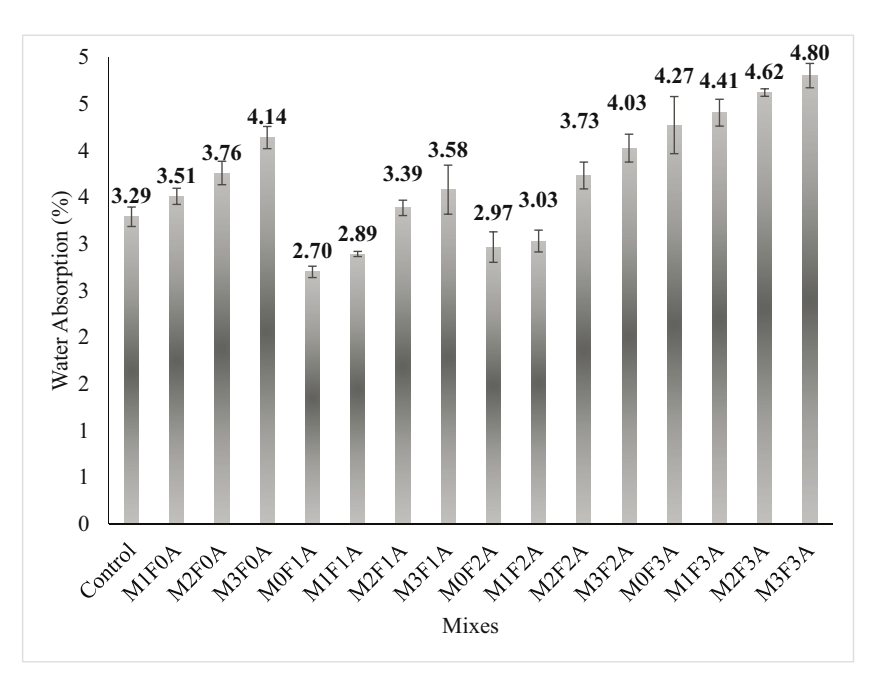


Figure 14: Water absorption results.

generated by the DPF. For instance, the microstructure of mix M1F1A is the most densified as seen in Figure 15c, followed by that of mix M2F2A. Furthermore, comparing Figure 15b and d, all of which contain 2% DPF, the microstructure of the latter is most densified and homogenous with fewer pores compared to that of the former. This densification is due to the filler ability of the NAC. Another reason is that it serves as a nucleation site effect for polymerization products beyond dissolution [42].

3.8.2 XRD analysis

XRD was conducted to examine the influence of the addition of NAC on the hydration reactions of cement paste in the DPFRC. Selective mixes containing different proportions of DPF and NAC were chosen and tested using XRD. The results of the XRD analysis are presented in Figure 16a–c. In the XRD results, Q represents quartz (SiO₂), C denotes calcite (CaCO₃), P denotes Portlandites, *i.e.*, Ca(OH)₂, and E represents ettringites. In all the figures, broad amorphous humps can be seen due to the formation of calcium silicate hydrate (C–S–H), which is accountable for the strength development and densification of the microstructure. The XRD patterns of all the mixes were similar showing alike peak patterns, with the

main hydration products being silica, Portlandites, calcites, and alumina. A very faint peak of ettringite was traced on some of the mixes at lower 2θ degrees. In the control, the main hydration product is Ca(OH)2, which has the highest peak intensity and several other peaks at different 2θ values, followed by silica and calcite. The presence of the Ca(OH)2 peak in the control is due to the hydration reaction between the cement compound (CaO) and water to form Ca(OH)₂ as a by-product. Comparable outcomes have been reported by previous studies [58]. The calcite in the control XRD might be due to the carbonization effect occurring during cement hydration [58,59]. For the mixes containing NAC, the main hydration product is the calcite (CaCO₃), which has the highest peak intensity and occurs at several 2θ degrees. This is occurring due to the presence of a high proportion of carbon in the NAC; the carbon reacts with the CaO in cement to form calcium carbonate. The addition of the NAC decreased the Portlandite content in the concrete, which can be seen by comparing the peaks of Ca(OH)2 in the control with the peaks of Ca(OH)₂ in the mixes with NAC (Figure 16b and c). The mix with the highest NAC content (M3F3A) has the highest peak intensity for CaCO₃. As part of the CaO in the cement is reacting with the carbon from NAC, this led to the reduction in the generation of unreacted Ca(OH)2. This might be one of the reasons for

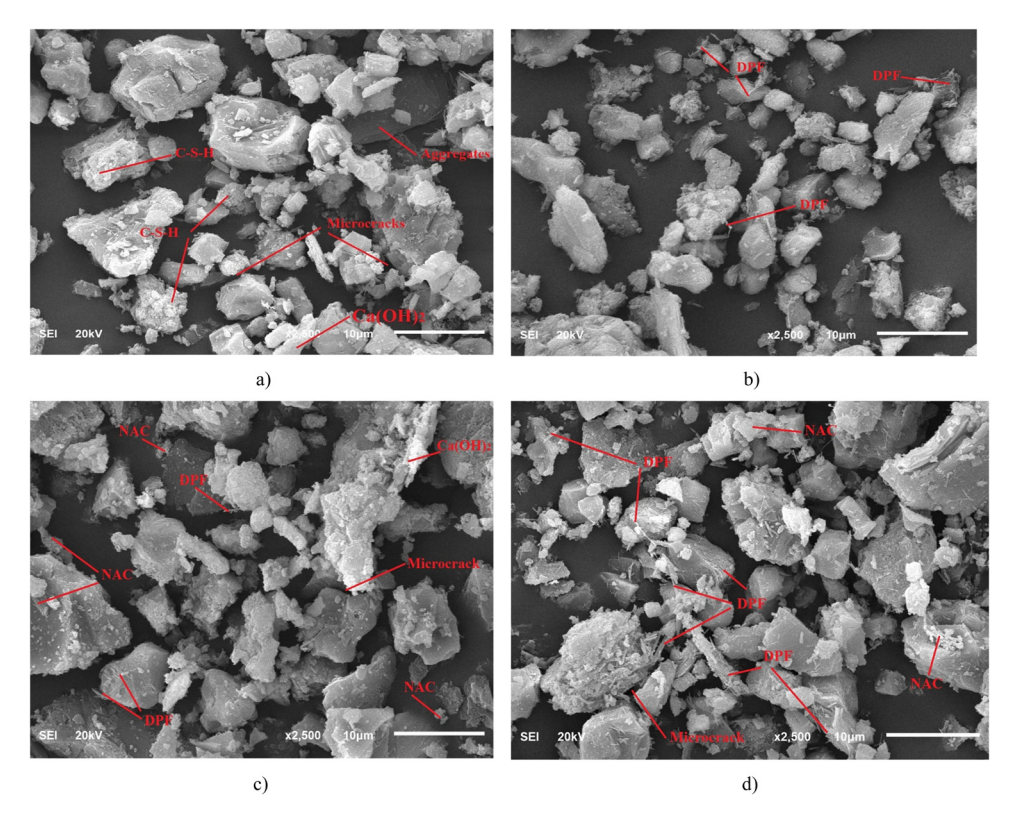


Figure 15: SEM images of DPFRC mixes. (a) Control, (b) M2F0A, (c) M1F1A, and (d) M2F2A.

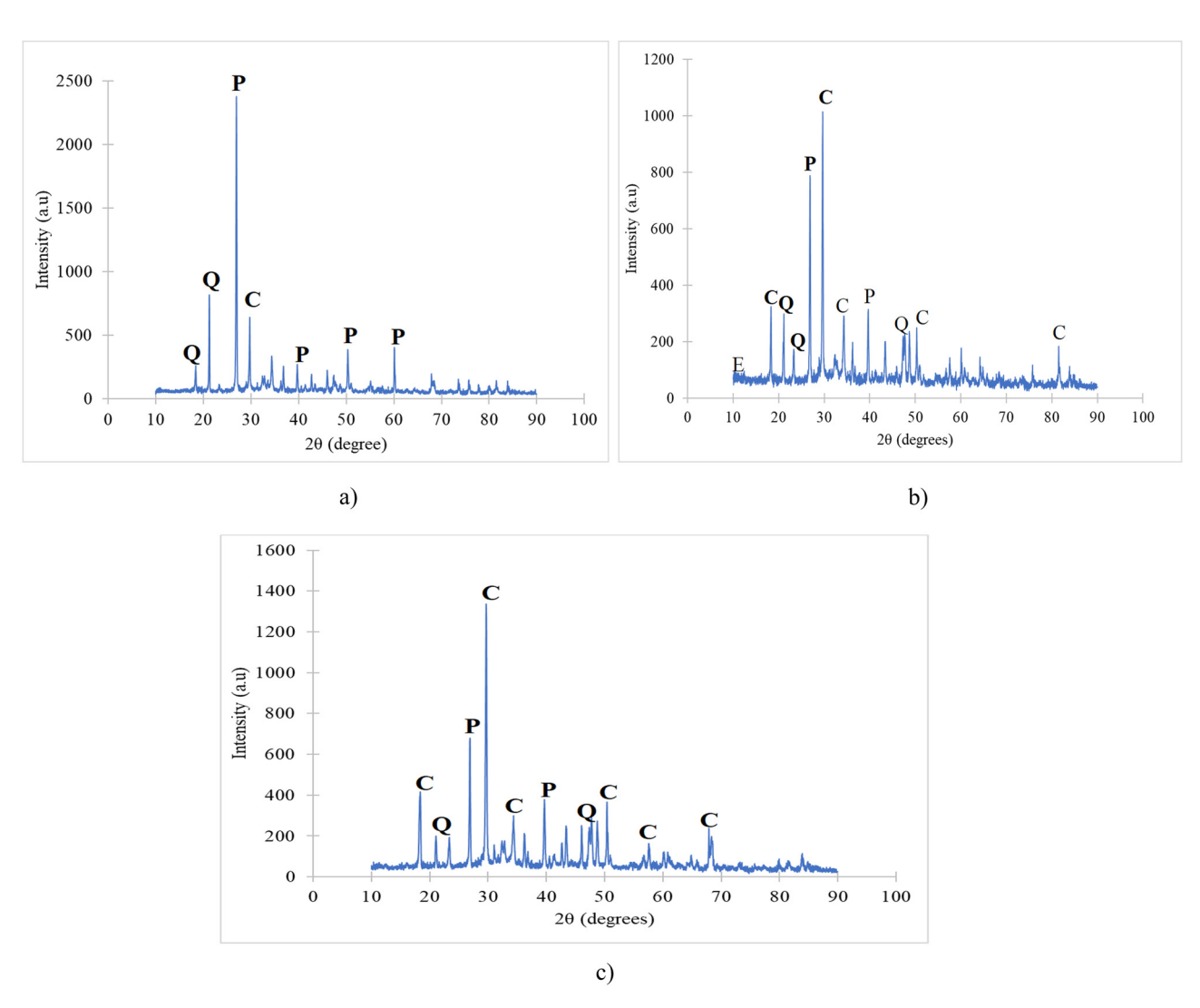


Figure 16: XRD pattern of DPFRC mixes. (a) Control, (b) mix M2F2A, and (c) M3F3A.

the improvements in the strengths of the concrete with the addition of NAC.

3.9 Statistical modeling using multivariable regression

Statistical modeling using multivariable regression analysis (MRA) was conducted to establish mathematical equations for the prediction of the properties of the DPFRC containing DPD and NAC as variables. Based on the experimental results, prediction models for the slump, fresh density, strengths, and water absorption were established.

The basic globalized MRA equation is expressed in the form of a linear equation as shown in Eq. (1) [60]:

$$y(x_1, x_2, x_3, ..., x_n) = \psi + \delta_1 x_1 + \delta_2 x_2 + \delta_3 x_3 + ... + \delta_n x_n,$$
 (1)

where y denotes the response/output, ψ is the coefficient of the intercept, and δ is the linear regression coefficient.

However, as most of the relationships between the responses/outputs and variables contain some curvature, a non-linear multi-variable regression analysis using second-order polynomials will improve the prediction accuracy and reduce the errors in the models. The global second-order non-linear MRA equation is expressed as Eq. (2) [60]:

$$y = \sum_{i=1}^{n} \delta_i x_i + \sum_{i=1}^{n-1} \sum_{j=i+1}^{n} \delta_{ij} x_i x_j + \psi,$$
 (2)

where y represents the response/output, x represents the independent variables, δ_i and δ_{ij} represent the coefficients of the first- and second-order polynomials, respectively, n is the number of input variables, and ψ is the constant of regression.

Table 5: ANOVA summary for multivariable regression models

Output/model	SS	MS	SE	<i>F</i> -value	<i>P</i> -value	Adj R ²	Pearson's R	R^2
Slump (mm)	1493.939	298.788	2.25	59.234	0.000014	0.960	0.988	0.977
Fresh density (kg/m³)	78589.51	15717.9	32.60	14.789	0.00133	0.852	0.956	0.913
7-day compressive strength (MPa)	679.962	135.992	2.34	24.799	0.00026	0.908	0.973	0.947
28-day compressive strength (MPa)	803.312	160.662	2.62	23.317	0.000314	0.903	0.971	0.943
7-day split tensile strength (MPa)	1.435	0.287	0.11	22.450	0.000355	0.899	0.970	0.941
28-day split tensile strength (MPa)	2.175	0.435	0.20	11.152	0.00314	0.809	0.943	0.90
7-day flexural strength (MPa)	3.316	0.663	0.15	28.279	0.000167	0.919	0.976	0.952
28-day flexural strength (MPa)	4.903	0.981	0.27	13.292	0.00185	0.837	0.951	0.905
Water absorption (%)	5.754	1.151	0.15	50.829	0.000024	0.954	0.987	0.973

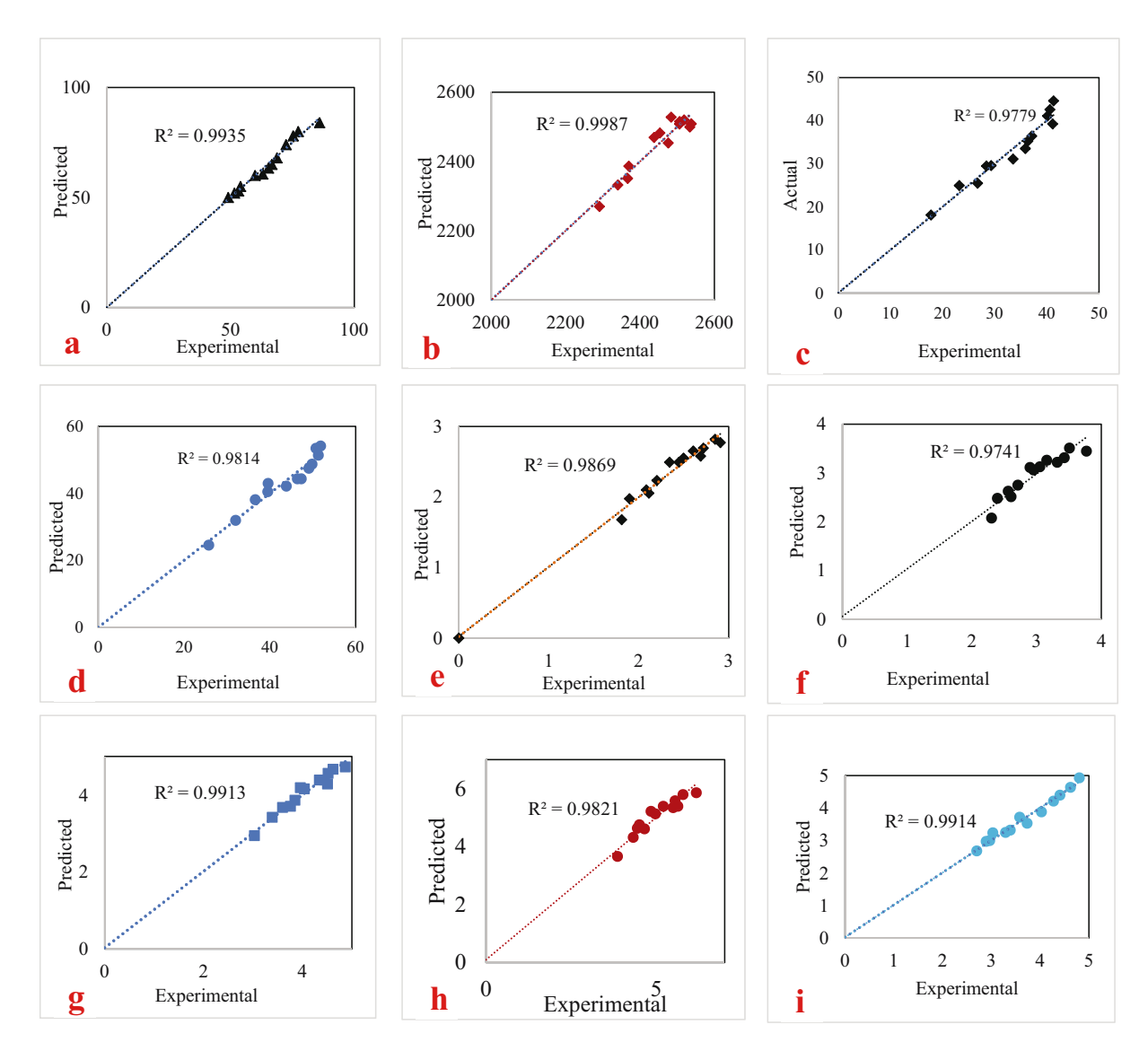


Figure 17: Predicted *versus* experimental (actual) plots for (a) Slump, (b) Density, (c) 7-day Compressive Strength, (d) 28-day Compressive Strength, (e) 7-day Split Tensile Strength, (f) 28-day Split Tensile Strength, (g) 7-day Flexural Strength, (h) 28-day Flexural Strength and (i) Water absorption models.

Therefore, in this study, non-linear MRA was adopted for the establishment of the model equations. The developed MRA equations for the fresh and hardened properties of the DPFRC are expressed as Eqs. (3)–(11):

$$S = 86 - 7.64 \times P - 2.20 \times D + 0.60 \times P \times D$$
$$-1.0 \times P^2 + 0.42 \times D^2,$$
 (3)

$$D = 2453.63 + 134.82 \times P + 19.15 \times D - 3.50 \times P \times D$$
$$- 54.25 \times P^2 - 11.67 \times D^2,$$
 (4)

$$C_7 = 41.11 - 1.35 \times P + 2.82 \times D - 1.19 \times P \times D$$

- $1.86 \times P^2 + 0.93 \times D^2$.

$$C_{28} = 49.85 + 3.10 \times P + 3.94 \times D - 2.01 \times P \times D$$

- $2.18 \times P^2 - 0.83 \times D^2$, (6)

$$\$_7 = 2.65 + 0.16 \times P + 0.25 \times D - 0.04 \times P \times D - 0.12 \times P^2 - 0.09 \times D^2,$$
 (7)

$$$_{28} = 3.26 + 0.20 \times P + 0.37 \times D - 0.04 \times P \times D - 0.15 \times P^2 - 0.13 \times D^2,$$
(8)

$$T_7 = 4.39 + 0.11 \times P + 0.55 \times D - 0.16 \times P \times D$$

- $0.11 \times P^2 - 0.11 \times D^2$. (9)

$$T_{28} = 5.39 + 0.12 \times P + 0.76 \times D - 0.19 \times P \times D$$

$$- 0.13 \times P^2 - 0.17 \times D^2,$$
(10)

WA =
$$3.25 - 1.01 \times P + 0.32 \times D - 0.05 \times P \times D + 0.44 \times P^2 - 0.03 \times D^2$$
, (11)

where S is the slump in mm; D is the fresh density in kg/m³; C_7 and C_{28} are the 7- and 28-compressive strengths, respectively, in MPa; $\$_7$ and $\$_{28}$ are the 7- and 28-day split tensile strengths, respectively, in MPa; T_7 and T_{28} are the 7- and 28-flexural strengths, respectively, in MPa; T_7 and T_7 is the water absorption in T_7 and T_7 and T_7 and T_7 is the water absorption in T_7 and T_7 and T_7 and T_7 is the water absorption in T_7 and T_7 and T_7 and T_7 is the water absorption in T_7 and T_7 and T_7 and T_7 is the water absorption in T_7 and T_7 and T_7 is the water absorption in T_7 and T_7 and T_7 is the water absorption in T_7 and T_7 and T_7 is the water absorption in T_7 and T_7 and T_7 is the water absorption in T_7 and T_7 and T_7 is the water absorption in T_7 and T_7 and T_7 is the water absorption in T_7 and T_7 and T_7 is the water absorption in T_7 and T_7 and T_7 is the water absorption in T_7 and T_7 and T_7 and T_7 is the water absorption in T_7 and T_7 and T_7 and T_7 and T_7 are the T_7 and T_7 and T_7 and T_7 are the T_7 and T_7 and T_7 and T_7 are the T_7 and T_7 are the T_7 and T_7 are the T_7 and T_7 and T_7 are the T_7 and T_7 are the T_7 are the

Table 5 highlights the ANOVA for all the models established for the estimation of the DPFRC's properties. Using the level of significance (P < 0.05), the statistical significance for all the models was checked. All the models were found to be statistically significant based on the significance test (P < 0.05), as their P-values are less than 0.05. Hence, the statistical null hypotheses for all the models were false and rejected. In the established models, scripts P < 0.05, the statistical significance of each of the models was tested. Higher values of P < 0.05 implied a high degree of correlation of the models with the experimental results and hence high predicting accuracy. As shown in Table 5, all models have excellent P < 0.05. Therefore, the

developed equations can be used to estimate the properties of the DPFRC with high precision.

The predicted responses against the experimental (actual) data were plotted to explain and show the predicting accuracy and correlation of the models graphically (Figure 17a–i). All the models have a very good correlation with the experimental results, as shown by the data points fitting well along the straight trend lines. The plots between the predicted responses (properties) and the experimental (actual) data for all the models have R^2 values ranging between 99.9 and 97.4%. The plots only between 0.1 and 2.6% of the data points were not fully correlated for all the models. The plot for fresh density has the highest correlation of 99.9%, while the plots for 28-day split tensile strength have the lowest correlation of 97.4%.

4 Conclusions

In this research, the impact of DPF and NAC on the fresh and hardened properties of DPFRC was examined. The derived conclusions are as follows:

- The addition of both DPF and NAC to the DPFRC concrete led to a reduction in the workability of the concrete, which was measured using the slump test. Hence, DPF and NAC decreased the consistency of the concrete.
- 2) The addition of DPF to the DPFRC resulted in a decrease in its densities at both fresh and hardened states. On the other hand, the addition of up to 2% NAC by cement weight to the DPFRC resulted in an increase in its densities at both fresh and hardened states.
- 3) The addition of DPF to the DPFRC led to a decrease in its compressive strength at all ages, where the decrease in strength was more significant with the addition of higher content of DPF.
- 4) The addition of 1% NAC by cement weight enhanced the DPFRC's compressive strength with or without DPF. Moreover, 1% NAC was successful in mitigating the loss in the compressive strength in the DPFRC with up to 2% fiber volume.
- 5) The incorporation of up to 2% DPF led to improvements in the flexural and split tensile strengths of the DPFRC.
- 6) The addition of up to 1% NAC led to further enrichment in the split tensile and flexural strengths of the DPFRC. Further, 1% NAC mitigated the loss in tensile and flexural strengths due to the addition of 3% DPF to the DPFRC.
- 7) The rate of water absorption of the DPFRC increased with the increase in the DPF volume. The addition of

- up to 2% NAC led to a decrease in the water absorption of the DPFRC.
- 8) The addition of up to 2% NAC densified the microstructure of the DPFRC by refining and filling the pores generated by the DPF.
- 9) The multi-variable statistical models developed to estimate the mechanical properties of the DPFRC containing DPF and NAC were very significant with a superb degree of precision.

Acknowledgments: The authors wish to acknowledge the support of the Structures and Materials Laboratory (S&M Lab) of the College of Engineering, Prince Sultan University, Riyadh, Saudi Arabia, for their vital support. The authors also wish to acknowledge the support of Prince Sultan University for paying the Article Processing Charges (APC) of this publication.

Funding information: The support of Prince Sultan University for paying the Article Processing Charges (APC).

Author contributions: Musa Adamu: conceptualization, methodology, investigation, formal analysis, writing – original draft; Yasser E. Ibrahim: resources, supervision, writing – review and editing; Omar Shabbir Ahmed: methodology, investigation, resources, writing – review and editing; Qasem A. Drmosh: methodology, investigation, analysis, writing – review and editing. All authors have accepted responsibility for the entire content of this manuscript and approved its submission.

Conflict of interest: The authors state no conflict of interest.

References

- [1] Al-Oqla FM, Sapuan S. Natural fiber reinforced polymer composites in industrial applications: feasibility of date palm fibers for sustainable automotive industry. J Clean Prod. 2014;66:347–54.
- [2] Makul N. Advanced smart concrete-A review of current progress, benefits and challenges. J Clean Prod. 2020;274:122899.
- [3] Gagg CR. Cement and concrete as an engineering material: An historic appraisal and case study analysis. Eng Fail Anal. 2014;40:114–40.
- [4] Chun B, Shin W, Jang YS, Yoo D-Y. Developing strain-hardening ultra-rapid-hardening mortar containing high-volume supplementary cementitious materials and polyethylene fibers. J Mater Res Technol. 2021;13:1934–45.
- [5] Aslam F, Zaid O, Althoey F, Alyami SH, Qaidi SM, de Prado Gil J, et al. Evaluating the influence of fly ash and waste glass on the characteristics of coconut fibers reinforced concrete. Struct Concr. 2022;24(2):2440–59.

- [6] Zaid O, Ahmad J, Siddique MS, Aslam F, Alabduljabbar H, Khedher KM. A step towards sustainable glass fiber reinforced concrete utilizing silica fume and waste coconut shell aggregate. Sci Rep. 2021;11(1):1–14.
- [7] Zaid O, Ahmad J, Siddique MS, Aslam F. Effect of incorporation of rice husk ash instead of cement on the performance of steel fibers reinforced concrete. Front Mater. 2021;8:665625.
- [8] Ibrahim YE, Adamu M, Marouf ML, Ahmed OS, Drmosh Q, Malik MA. Mechanical performance of date-palm-fiber-reinforced concrete containing silica fume. Buildings. 2022;12(10):1642.
- [9] Adamu M, Alanazi F, Ibrahim YE, Alanazi H, Khed VC. A comprehensive review on sustainable natural fiber in cementitious composites: The date palm fiber case. Sustainability. 2022;14(11):6691.
- [10] Danish A, Mosaberpanah MA, Salim MU, Amran M, Fediuk R, Ozbakkaloglu T, et al. Utilization of recycled carbon fiber reinforced polymer in cementitious composites: A critical review. J Build Eng. 2022:53:104583
- [11] Ozerkan NG, Ahsan B, Mansour S, Iyengar SR. Mechanical performance and durability of treated palm fiber reinforced mortars. Int J Sustain Built Environ. 2013;2(2):131–42.
- [12] Bentur A, Mindess S. Fibre reinforced cementitious composites. New York, United States of America: CRC Press; 2006.
- [13] Li Z, Wang X, Wang L. Properties of hemp fibre reinforced concrete composites. Compos part A: Appl Sci Manuf. 2006;37(3):497–505.
- [14] Kalia S, Avérous L, Njuguna J, Dufresne A, Cherian BM. Natural fibers, bio-and nanocomposites. Int J Polym Sci. 2011;2011. https://doi.org/10.1155/2011/735932.
- [15] Faruk O, Bledzki AK, Fink H-P, Sain M. Biocomposites reinforced with natural fibers: 2000–2010. Prog Polym Sci. 2012;37(11):1552–96.
- [16] Bamaga S. A review on the utilization of date palm fibers as inclusion in concrete and mortar. Fibers. 2022;10(4):35.
- [17] Lahouioui M, Ben Arfi R, Fois M, Ibos L, Ghorbal A. Investigation of fiber surface treatment effect on thermal, mechanical and acoustical properties of date palm fiber-reinforced cementitious composites. Waste Biomass Valoriz. 2020;11(8):4441–55.
- [18] Kriker A, Debicki G, Bali A, Khenfer M, Chabannet M. Mechanical properties of date palm fibres and concrete reinforced with date palm fibres in hot-dry climate. Cem Concr Compos. 2005;27(5):554–64.
- [19] Khelifa H, Bezazi A, Boumediri H, del Pino GG, Reis PN, Scarpa F, et al. Mechanical characterization of mortar reinforced by date palm mesh fibers: Experimental and statistical analysis. Constr Build Mater. 2021;300:124067.
- [20] Mahoutian M, Lubell AS, Bindiganavile VS. Effect of powdered activated carbon on the air void characteristics of concrete containing fly ash. Constr Build Mater. 2015;80:84–91.
- [21] Moses MT, Thomas LB, Scaria J, Dev GV. Prospective benefits of using activated carbon in cement composites - An overview. Technology. 2019;10(4):946–53.
- [22] Morgan B, Dumbauld G. Use of activated charcoal in cement to combat effects of contamination by drilling muds. J Pet Technol. 1952;4(9):225–32.
- [23] Justo-Reinoso I, Srubar WV III, Caicedo-Ramirez A, Hernandez MT. Fine aggregate substitution by granular activated carbon can improve physical and mechanical properties of cement mortars. Constr Build Mater. 2018;164:750–9.
- [24] Horgnies M, Dubois-Brugger I, Gartner E. NOx de-pollution by hardened concrete and the influence of activated charcoal additions. Cem Concr Res. 2012;42(10):1348–55.

- [25] Krou N, Batonneau-Gener I, Belin T, Mignard S, Horgnies M, Dubois-Brugger I. Mechanisms of NOx entrapment into hydrated cement paste containing activated carbon – Influences of the temperature and carbonation. Cem Concr Res. 2013;53:51–8.
- [26] Erşan YÇ, Da Silva FB, Boon N, Verstraete W, De Belie N. Screening of bacteria and concrete compatible protection materials. Constr Build Mater. 2015;88:196–203.
- [27] Resheidat M, Al-Araji N, Ghanma M, editors. Effect of charcoal on the porosity and the properties of concrete. Innovations and Developments in Concrete Materials and Construction: Proceedings of the International Conference held at the University of Dundee, Scotland, UK on 9–11 September 2002. Thomas Telford Publishing; 2002.
- [28] Krou N, Batonneau-Gener I, Belin T, Mignard S, Javierre I, Dubois-Brugger I, et al. Reactivity of volatile organic compounds with hydrated cement paste containing activated carbon. Build Environ. 2015:87:102–7
- [29] Elmouwahidi A, Zapata-Benabithe Z, Carrasco-Marín F, Moreno-Castilla C. Activated carbons from KOH-activation of argan (Argania spinosa) seed shells as supercapacitor electrodes. Bioresour Technol. 2012;111:185–90.
- [30] Na S, Lee S, Youn S. Experiment on activated carbon manufactured from waste coffee grounds on the compressive strength of cement mortars. Symmetry. 2021;13(4):619.
- [31] Zheng C, Liu Z, Xu J, Li X, Yao Y. Compressive strength and microstructure of activated carbon-fly ash cement composites. Chem Eng Trans. 2017;59:475–80.
- [32] Wang Y, Ge Y, Wang X, Chen X, Li Q. The effect of powder activated carbon on mechanical properties and pore structures of cementbased mortars. Constr Build Mater. 2022;316:125798.
- [33] ASTM C150/150M. Standard specification for Portland cement. West Conshohocken, PA, USA: ASTM International; 2015.
- [34] ASTM C33. Standard specification for concrete aggregates. West Conshohocken, PA, USA: ASTM International; 2018.
- [35] ACI 211.1R. Standard practice for selecting proportions for normal, heavyweight, and mass concrete. Michigan, USA: American Concrete Institute; 2002.
- [36] Adamu M, Ibrahim YE, Abdel daiem MM, Alanazi H, Elalaoui O, Ali NM. Optimization and modelling the mechanical performance of date palm fiber-reinforced concrete incorporating powdered activation carbon using response surface methodology. Materials. 2023;16(8):2977.
- [37] ASTM C143/C143M. Standard test method for slump of hydrauliccement concrete. West Conshohocken, PA, USA: ASTM International; 2012.
- [38] ASTM C138/C138M. Standard test method for density (Unit Weight), yield, and air content (Gravimetric) of concrete. West Conshohocken, PA, USA: ASTM International; 2017.
- [39] BS EN 12390-3. Testing hardened concrete. Compressive strength of test specimens. London, United Kingdom: British Standards Institution; 2009.
- [40] ASTM C78/C78M. Standard test method for flexural strength of concrete (Using Simple Beam with Third-Point Loading). West Conshohocken, PA, USA: ASTM International; 2015.
- [41] Lekkam M, Benmounah A, Kadri E-H, Soualhi H, Kaci A. Influence of saturated activated carbon on the rheological and mechanical properties of cementitious materials. Constr Build Mater. 2019;198:411–22.
- [42] Rashad AM, Said N, Abdel-Gawwad HA. An initial study about the effect of activated carbon nano-sheets from residual biomass of

- olive trees pellets on the properties of alkali-activated slag pastes. | Build Eng. 2021;44:102661.
- [43] Zaid O, Hashmi SRZ, Aslam F, Abedin ZU, Ullah A. Experimental study on the properties improvement of hybrid graphene oxide fiber-reinforced composite concrete. Diam Relat Mater. 2022;124:108883.
- [44] Ali-Boucetta T, Ayat A, Laifa W, Behim M. Treatment of date palm fibres mesh: Influence on the rheological and mechanical properties of fibre-cement composites. Constr Build Mater. 2021;273:121056.
- [45] Adamu M, Trabanpruek P, Jongvivatsakul P, Likitlersuang S, Iwanami M. Mechanical performance and optimization of highvolume fly ash concrete containing plastic wastes and graphene nanoplatelets using response surface methodology. Constr Build Mater. 2021;308:125085.
- [46] Kriker A, Bali A, Debicki G, Bouziane M, Chabannet M. Durability of date palm fibres and their use as reinforcement in hot dry climates. Cem Concr Compos. 2008;30(7):639–48.
- [47] Boumhaout M, Boukhattem L, Hamdi H, Benhamou B, Nouh FA. Thermomechanical characterization of a bio-composite building material: Mortar reinforced with date palm fibers mesh. Constr Build Mater. 2017;135:241–50.
- [48] Maglad AM, Zaid O, Arbili MM, Ascensão G, Şerbănoiu AA, Grădinaru CM, et al. A study on the properties of geopolymer concrete modified with nano graphene oxide. Buildings. 2022;12(8):1066.
- [49] Benaniba S, Driss Z, Djendel M, Raouache E, Boubaaya R. Thermomechanical characterization of a bio-composite mortar reinforced with date palm fiber. J Engineered Fibers Fabr. 2020;15:1558925020948234.
- [50] Committee A, editor. Building code requirements for structural concrete (ACI 318-08) and commentary. American Concrete Institute; 2008.
- [51] Béton CE-Id. CEB-FIP model code 1990: Design code. Thomas Telford Publishing; 1993.
- [52] ACI 363. Report on high-strength concrete. Michigan, USA: American Concrete Institute; 2010.
- [53] Hesami S, Modarres A, Soltaninejad M, Madani H. Mechanical properties of roller compacted concrete pavement containing coal waste and limestone powder as partial replacements of cement. Constr Build Mater. 2016;111:625–36.
- [54] Ahmed M, Hadi KME, Hasan MA, Mallick J, Ahmed A. Evaluating the co-relationship between concrete flexural tensile strength and compressive strength. Int J Struct Eng. 2014;5(2):115–31.
- [55] BS 8110-1. Structural use of concrete Code of practice for design and construction. London, United Kingdom: British Standard Institution; 1997.
- [56] Bamaga S. Physical and mechanical properties of mortars containing date palm fibers. Mater Res Express. 2022;9(1):015102.
- [57] Benmansour N, Agoudjil B, Gherabli A, Kareche A, Boudenne A. Thermal and mechanical performance of natural mortar reinforced with date palm fibers for use as insulating materials in building. Energy Build. 2014;81:98–104.
- [58] Liu S, Yan P. Effect of limestone powder on microstructure of concrete. J Wuhan Univ Technol-Mater Sci Ed. 2010;25(2):328–31.
- [59] Adamu M, Ibrahim YE, Al-Atroush ME, Alanazi H. Mechanical properties and durability performance of concrete containing calcium carbide residue and nano silica. Materials. 2021;14(22):6960.
- [60] Liu B, Shi J, Zhou F, Shen S, Ding Y, Qin J. Effects of steam curing regimes on the capillary water absorption of concrete: Prediction using multivariable regression models. Constr Build Mater. 2020;256:119426.